Communication

Room-temperature Formation of Hollow Cu_2O Nanoparticles

By *Ling-I Hung*, *Chia-Kuang Tsung*, *Wenyu Huang*, and *Peidong Yang**

[*] Prof. P. Yang, Dr. L.-I. Hung, Dr. C.-K. Tsung, Dr. W. Huang
Department of Chemistry
University of California–Berkeley
Berkeley, 94720 CA (USA)
E-mail: p_yang@berkeley.edu
Dr. L.-I. Hung
Materials and Chemical Laboratories
Industrial Technology Research Institute
195, Sec. 4, Chung Hsing Road, Chutung, Hsinchu, 310 (Taiwan, R.O.C.)

[**] L.-I. H and C.-K. T contributed equally to this work. This work was supported by the Director, Office of Basic Energy Sciences, Materials Sciences and Engineering Division, of the U.S. Department of Energy under Contract No. DE-AC02-05CH11231 and supported by ITRI Project 7C29KT1541 under sponsorship of the Ministry of Economic Affairs, Taiwan, R.O.C.

Abstract

Monodisperse Cu and Cu_2O nanoparticles (NPs) were synthesized non-hydrolytically using tetradecylphosphonic acid as a capping agent. Dispersing the NPs in chloroform and hexane at room temperature resulted in the formation of hollow Cu_2O NPs and $Cu@Cu_2O$ core-shell NPs, respectively. Transmission electron microscopy, X-ray diffraction, and UV-vis absorption spectroscopy were used to systematically study the oxidation of the nanoparticles. The monodisperse Cu_2O nanoparticles were used to fabricate hybrid bilayer solar cells with efficiency of 0.14% under AM 1.5 and 1 Sun illumination.

The synthesis of colloidal nanoparticles (NPs) possessing hollow or core-shell structures has attracted a great deal of attention because these materials exhibit unique physical and chemical properties that allow them to be used in catalysis and drug delivery.[1-4] These particles are typically produced using sacrificial templates, such as polystyrene or silica. Nevertheless, this templating strategy often limits the core size to within a few hundred nanometers. In 2004, Yin *et al.* demonstrated the first preparation of hollow CoO NPs through the oxidation of Co NPs, using the concept of the nanoscale Kirkendall effect.[5] Since then, many hollow and core-shell nanocrystals of oxides and chalcogenides have been synthesized this way.[6-10] Colloidal synthesis of metal NPs accompanied by the Kirkendall process often produces high yields of monodisperse hollow nanoparticles. The synthesis of hollow metal oxide nanocrystals usually involves two distinct processes: surface oxidation (resulting in the formation of core-shell nanostructures) and vacancy coalescence induced by outward diffusion of the metal atoms (resulting in the formation of hollow structures). Metals such as Fe, Cu, Al, and Zn undergo surface oxidation when they are exposed to ambient atmosphere at room temperature. Further oxidation is prohibited by the surface oxide layer, the thickness of which is usually on the order of several nanometers. The formation of hollow nanocrystals is often performed in solution phase at elevated temperatures to accelerate the outward diffusion of metal ions from the core. Only a few examples of hollow metal oxide nanospheres formed at low temperature have been reported.[6, 11]

The oxidation of Cu NPs[12] is interesting to study because Cu possesses multiple oxidation states and usually forms the stable oxides, Cu_2O and CuO. The $Cu/Cu_2O/CuO$ system has been applied to facilitate oxidation reactions in the bulk; as a result, it might

be useful as an alternative for noble metals in various catalytic systems. Cu_2O is an environmentally friendly p-type semiconductor having a band gap of 2 eV and a high optical absorption coefficient, making it an excellent candidate for solar energy conversion applications.[13] The shape-controlled synthesis of Cu_2O micro- and nanocrystals has been explored to conduct the fabrication process in the potential application.[14, 15] With high surface area and low material density, hollow NPs are one important class of those nanocrystals. Several hollow Cu_2O nanocrystals with defined interior architectures have been prepared previously through the dry oxidation of Cu NPs[11] or the reduction of self-assembled CuO particles.[16] Furthermore, the high diffusion rate of Cu in copper oxides makes it an ideal material for studying the Kirkendall effect.[17] In this work, we describe the solution-phase synthesis of highly monodisperse Cu NPs and, by controlling the oxidation process, the formation of $Cu@Cu_2O$ core-shell structures, hollow Cu_2O nanospheres, and solid Cu_2O nanospheres.

We synthesized the Cu NPs through the thermal decomposition of copper(I) acetate (CuOAc) in trioctylamine (TOA) in the presence of tetradecylphosphonic acid (TDPA), forming a purplish-red colloidal solution. The dark-red NPs were precipitated by adding ethanol and were collected through centrifugation. The NPs were readily dispersed in organic solvents, including hexane and chloroform. Analysis using transmission electron microscopy (TEM) indicated that the presence of TDPA, a strongly binding capping agent[18], led to the formation of monodisperse Cu nanospheres (Fig. 1, a and b). The average size of the Cu nanoparticles was 8.4 (± 0.8) nm. The narrow size distribution was demonstrated from the formation of a large-area close-packed array of Cu NPs on the TEM grid after evaporation of the solvent (Fig. 1a). No size-selection

steps were applied before the array formation. Changing the molar ratio of TDPA to the Cu precursor allowed us to tune the size of the Cu nanoparticles. For example, we obtained larger Cu NPs (average size: 14.7 nm) when the TDPA/CuOAc ratio was increased to 1 (Fig. 1c).

To study the oxidation of the nanostructures, we dispersed the NPs in hexane and chloroform under ambient conditions. Both of these NP solutions appeared reddish green in color immediately after dispersing the particles. The color of each solution gradually changed to forest green. The green color of the hexane solution persisted for several months, whereas the chloroform solution turned yellow after a few hours under ambient conditions. We used TEM and X-ray diffraction (XRD) to examine the nanostructural transformations of the NPs in both solutions during the oxidation process. TEM images of the oxidized products prepared from hexane (Fig. 1d) and chloroform (Fig. 1e) revealed core-shell and hollow spherical structures, respectively. They also indicated that the monodispersity of the nanoparticles was maintained during the oxidation. High-resolution TEM (HRTEM) images revealed that the as-prepared nanoparticles had five-fold symmetry and possessed a very thin surface layer that featured a different spacing from that of the core (Fig. 1f). The lattice plane distance of the core was 0.21 nm, corresponding to the (111) plane of face-centered cubic (fcc) Cu. The thickness of the outer layer increased with increasing time after dispersion in the solvents; after 12 h, a Cu_2O film having a thickness of ca. 2.5 nm was formed (Fig. 1g). At this stage, the NPs suspended in hexane retained their core-shell structure, whereas those dispersed in chloroform transformed further into single-crystal or polycrystalline hollow NPs (Fig. 1h and S1).

Solid Cu_2O NPs were obtained after altering the oxidation process. To induce further oxidation of the Cu@Cu_2O core-shell spherical NPs without forming hollow structures, Cu@Cu_2O NPs were deposited on a substrate and annealed at 200 °C. Fig. 1i displays the resulting solid Cu_2O spheres. The XRD patterns (Fig. 2) were consistent with the HRTEM images. The peaks in the XRD pattern of the as-prepared NPs can be indexed to the fcc structure of Cu (Fm-3m; a = 3.615; JCPDF no. 85-1326), with the weak peak at ca. 42.5° corresponding to the (111) plane of Cu_2O. Upon increasing the dispersion time, the peaks of the Cu_2O phase increased in intensity, whereas those of the Cu phase decreased in intensity, consistent with the formation of the core-shell structure. XRD analysis also confirmed the presence of pure Cu_2O phases for both the hollow and solid NPs. These results from TEM and XRD analyses showed that we could control the Cu/Cu_2O structure within the NPs through controllable oxidation conditions (Scheme 1).

The surface oxidation of many metals occurs at a very rapid rate until the formation of an oxide layer prevents further exposure of the metal. According to Cabrera and Mott[19], low-temperature oxidation occurs through oxygen atoms adsorbing onto the oxide surface and then electrons penetrating into the oxide layer rapidly by tunneling to establish equilibrium between the metal and the adsorbed oxygen. This process results in the formation of an electric field in the thin oxide layer, which attracts metal ions. The diffusion of Cu ions to the surface of the NPs was evidenced by the slight increase in the average particle size (see Supporting Information, Fig. S2). Moreover, the retention of the TDPA capping group not only maintained the uniformity of the particle size but also affected the oxidation of the Cu NPs in the different solvents. Observed from solubility experiments, TDPA is relatively more soluble in chloroform than in hexane. It implies

that exposure of the Cu@Cu_2O NPs to dissolved oxygen in chloroform was higher. As a result, we observed the Kirkendall effect on the Cu@Cu_2O NPs only in the chloroform solution.

Analogous to the behavior of Au and Ag NPs, Cu NPs also exhibit size- and shape-dependent surface plasmon resonance (SPR) absorptions in the visible range.[20-22] The SPR absorptions of the as-synthesized 8- and 14-nm diameter Cu NPs were centered at 600 and 578 nm, respectively (Fig. 3a). The SPR peak of the 8-nm Cu NPs in chloroform (centered at 600 nm) gradually decreased in intensity over 24 h, whereas that of the Cu NPs in hexane (centered at 616 nm) remained pronounced over the same period of time. The SPR peak of the Cu NPs in hexane persisted, but shifted to 630 nm, after storing the solution in air for several months. This solvent-dependent oxidation evolution of 8-nm Cu NPs was studied by monitoring the SPR absorption. The SPR absorptions were *in-situ* measured every 15 min during the oxidation. The center wavelengths and absorption intensities of the SPR changed with time and were plotted as functions of time in Fig. 3, b and c, respectively. The red shifts in Fig. 3b, decreased absorption intensities in Fig. 3c, and widening bandwidths of these signals indicated that metallic Cu was depleted from the NPs. Our observed red shifts of the SPR peak for the Cu NPs as their sizes decreased is consistent with previous findings.[21, 22] The changes in the wavelength and intensity of the pronounced peak within the visible light range as a function of time clearly indicated that different structural transformations were occurring for the Cu NPs in the different solvents, consistent with our TEM and XRD analyses.

Since Cu_2O has a band gap of 2 eV and a high optical absorption coefficient, it represents one of the environmentally friendly semiconductors for solar energy

conversion applications. We have tested the possibility of using these monodisperse Cu_2O nanoparticles in hybrid solar cells. In this study [6, 6]-phenyl-C_{61}-butyric acid methyl ester (PCBM) was chosen as the electron acceptor to fabricate Cu_2O/PCBM bilayer solar cells. Cu_2O thin film was fabricated by spin-coating Cu@Cu_2O NPs on ITO-coated glass substrates followed by annealing to produce solid Cu_2O NPs. Fig. 4 shows *I-V* characteristics for a Cu_2O/PCBM cell with a 200 nm thickness of Cu_2O. The inset shows energy diagram of the device, with energy levels of ITO, Cu_2O, PCBM and Al.[23, 24] The thickness of the Cu_2O films was determined based on thin film optical absorption. Using a combination of UV-vis absorption, profilometry, and cross-sectional SEM measurements, we have calculated the optical absorption coefficient to be 6.6×10^4 cm^{-1} at 450 nm. We found that short-current current densities (J_{sc}) are highly dependent on the Cu_2O thickness as shown in Table 1. We believe that J_{sc} in these bilayer cells are largely regulated by charge carrier mobility and thickness-dependent light absorption. We were able to achieve best efficiency 0.14% under AM 1.5 and 1 Sun illumination.

In summary, we have developed a synthetic method for producing monodisperse Cu NPs and have investigated their oxidation behavior in different solvents at room temperature. By choosing a suitable solvent to control the oxidation process, we could prepare either hollow Cu_2O NPs or Cu@Cu_2O NPs selectively. Furthermore, we also obtained solid Cu_2O NPs through thermal treatment of the Cu@Cu_2O NPs at 200 °C. HRTEM and XRD analyses revealed the oxidation processes that occurred to the Cu NPs when exposed to dissolved oxygen in organic solvents at room temperature. We found that the nanoscale Kirkendall effect induced hollow Cu_2O NPs to form in chloroform as a result of the exposure of the NPs to dissolved oxygen because of the good solubility of

TDPA in chloroform. We anticipate that such solid and hollow Cu_2O NPs may find potential applications in solar energy conversion and catalysis.

Experimental

Synthesis: All chemicals are used as received without further purification. Copper NPs were prepared by decomposition of CuOAc in TOA in the presence of TDPA. In a typical synthesis, TOA (10 mL) was heated at 130 °C inside a three-neck flask for 30 min under flow of N_2 to remove water and dissolved O_2. After cooling to room temperature, 1 mmol CuOAc and 0.5 mmol TDPA were added with vigorous stirring. The solution was flushed with N_2, rapidly heated to 180 °C, maintained there for 30 min, rapidly heated to 270 °C, and then held there for an additional 30 min. The purplish red colloidal solution was cooled to room temperature by removing the flask from the oil bath. The colloidal solution was mixed with ethanol and the particles were precipitated through centrifugation at 6000 rpm for 15 min. The precipitate was redispersed in hexane and chloroform for further characterization. The dispersed NPs were drop-casted in silica coated TEM grid and Si chips for further experiments and characterizations. The thermal treatment is performed at 200°C in air or under low pressure (0.1 atm) with flow of oxygen.

Characterization: TEM micrographs were obtained using JEOL CX200 and FEI Tecnai G2 S-Twin electron microscopes (200 kV). TEM samples were prepared by placing a drop of the colloidal solution containing the NPs onto a carbon-coated Cu grid under ambient conditions. XRD analyses were performed using a Bruker AXS diffractometer, Co Kα radiation (1.790 Å) and a general area detector (GADDS, Bruker).

UV–Vis spectra were recorded for the NPs solubilized in hexane and chloroform using a SHIMADZU UV-3101PC UV–Vis–NIR scanning spectrometer.

Device processing and testing: $Cu@Cu_2O$ NPs in chloroform were spin-coated on ITO coated glass substrates and annealed at 200°C for 30 minutes. This step was repeated to produce Cu_2O films with varied thicknesses. PCBM dissolved in chloroform (10 mg/ml) was then spin-coated on the Cu_2O layer. The thickness of PCBM is 60 nm. Al contact regions (area = 0.03 cm^2, thickness = 100 nm) were deposited via thermal evaporation through a patterned shadow mask under high vacuum. Current-voltage measurements were performed in the dark and under AM 1.5 and 1 Sun illumination (Oriel, 300 W Model, 91160), with the incident light coming through the backside of the device.

Acknowledgements

This work was supported by the Director, Office of Basic Energy Sciences, Materials Sciences and Engineering Division, of the U.S. Department of Energy under Contract No. DE-AC02-05CH11231 and supported by ITRI Project 7C29KT1541 under sponsorship of the Ministry of Economic Affairs, Taiwan, R.O.C. Supporting Information is available online from the authors.

Received: ((will be filled in by the editorial staff))
Revised: ((will be filled in by the editorial staff))
Published online: ((will be filled in by the editorial staff))

Figure captions

Figure 1. TEM images of (a) a large-area view of the self-assembled Cu NPs, (b) the 8-nm Cu NPs, (c) the 14-nm Cu NPs, (d) the Cu@Cu_2O NPs, and (e) the hollow Cu_2O NPs; HRTEM images of the (f) Cu, (g) Cu@Cu_2O, (h) hollow Cu_2O, and (i) solid Cu_2O NPs.

Scheme 1. Oxidation of the Cu NPs to generate different monodisperse nanostructures.

Figure 2. Powder XRD patterns of the as-synthesized Cu, Cu@Cu_2O, hollow Cu_2O, and solid Cu_2O NPs.

Figure 3. (a) Absorbance spectra of Cu NPs of different sizes and structures. (b) SPR wavelengths and (c) intensities plotted as functions of time for NPs dispersed in hexane and chloroform. The inset shows the color of NPs dispersed in chloroform (yellow) and hexane (green) after UV-Vis measurement.

Figure 4. *I-V* characteristics of the ITO/Cu_2O(200nm)/PCBM/Al device in dark and under AM 1.5 and 1 Sun illumination. The inset shows the energy diagram of the device.

Table 1. Summary of the photovoltaic properties, V_{oc}, J_{sc}, F.F., and η for ITO/Cu_2O/PCBM/Al device with varied thickness of Cu_2O.

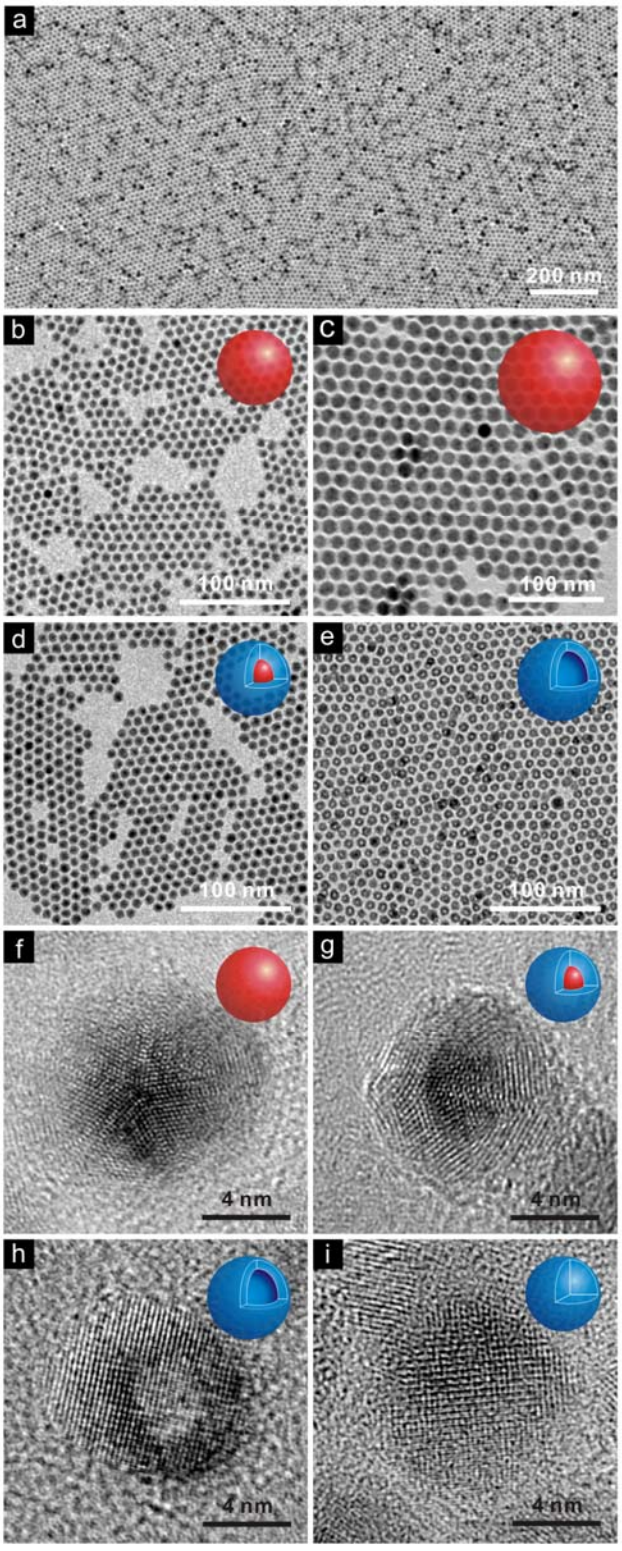

Fig. 1.

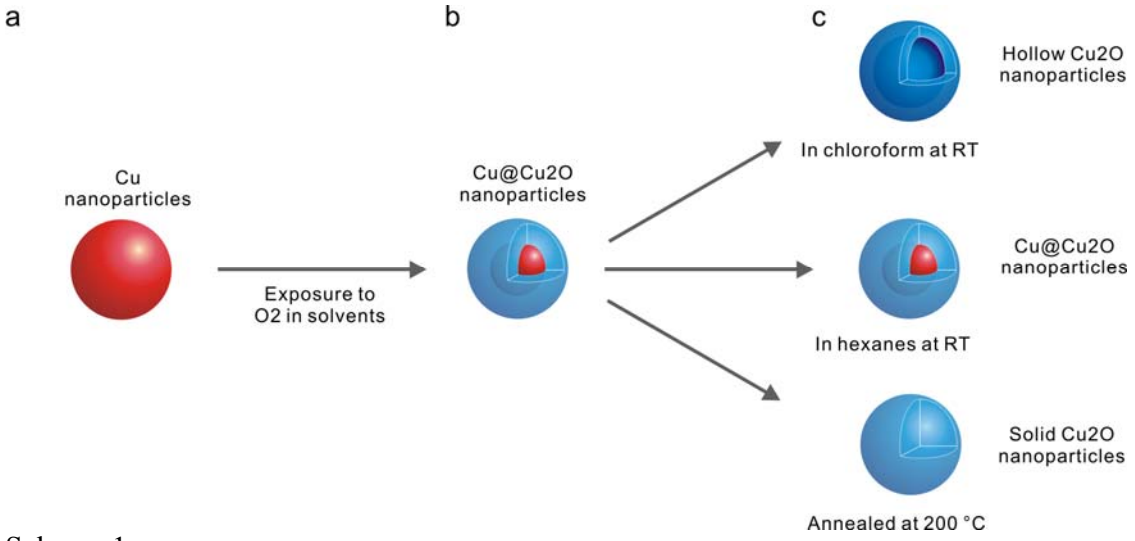

Scheme 1.

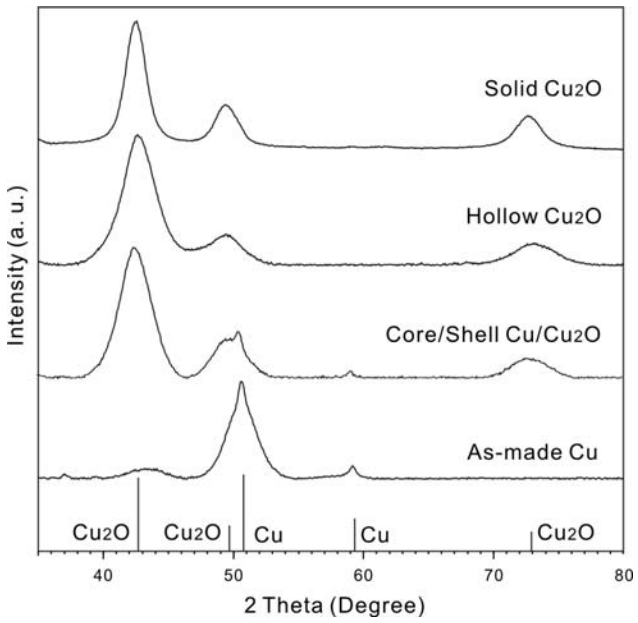

Fig. 2.

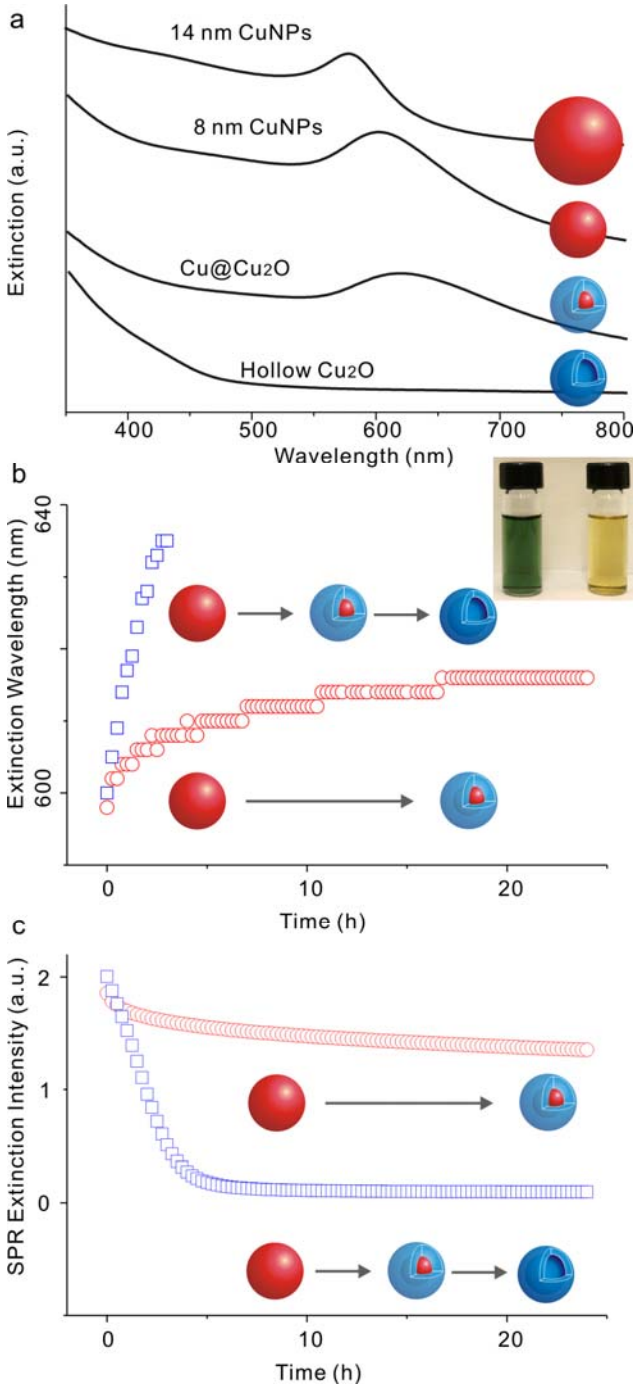
a
14 nm CuNPs
8 nm CuNPs
Cu@Cu2O
Hollow Cu2O
Extinction (a.u.)
400
500
600
700
800
Wavelength (nm)
b
Extinction Wavelength (nm)
640
600
0
10
20
Time (h)
c
SPR Extinction Intensity (a.u.)
2
1
0
0
10
20
Time (h)

Fig. 3.

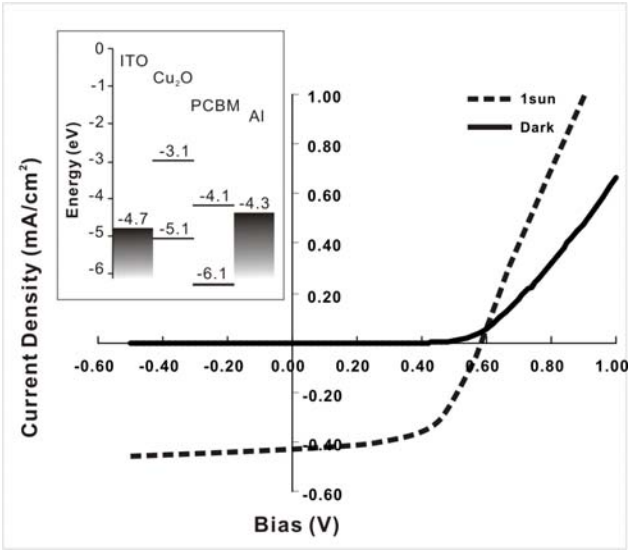

Fig 4.

Cu_2O Thickness (nm)	V_{oc} (V)	J_{sc} (mA/cm^2)	FF	η (%)
40	0.53	0.27	0.40	0.06
70	0.53	0.55	0.46	0.14
100	0.55	0.50	0.45	0.13
160	0.55	0.50	0.51	0.14
200	0.59	0.44	0.56	0.14

Table 1.

References

[1] O. D. Velev, E. W. Kaler, *Adv. Mater.* **2000**, *12*, 531.
[2] J. Erlebacher, M. J. Aziz, A. Karma, N. Dimitrov, K. Sieradzki, *Nature* **2001**, *410*, 450.
[3] S. H. Im, U. Y. Jeong, Y. N. Xia, *Nature Materials* **2005**, *4*, 671.
[4] F. Schuth, *Annual Review of Materials Research* **2005**, *35*, 209.
[5] Y. D. Yin, R. M. Rioux, C. K. Erdonmez, S. Hughes, G. A. Somorjai, A. P. Alivisatos, *Science* **2004**, *304*, 711.
[6] C. M. Wang, D. R. Baer, L. E. Thomas, J. E. Amonette, J. Antony, Y. Qiang, G. Duscher, *J. Appl. Phys.* **2005**, *98*, 094308.
[7] A. E. Henkes, Y. Vasquez, R. E. Schaak, *J. Am. Chem. Soc.* **2007**, *129*, 1896.
[8] S. Peng, S. H. Sun, *Angewandte Chemie-International Edition* **2007**, *46*, 4155.
[9] J. B. Fei, Y. Cui, X. H. Yan, W. Qi, Y. Yang, K. W. Wang, Q. He, J. B. Li, *Adv. Mater.* **2008**, *20*, 452.
[10] H. J. Fan, U. Gosele, M. Zacharias, *Small* **2007**, *3*, 1660.
[11] R. Nakamura, J. G. Lee, D. Tokozakura, H. Mori, H. Nakajima, *Mater. Lett.* **2007**, *61*, 1060.
[12] M. Yin, C. K. Wu, Y. B. Lou, C. Burda, J. T. Koberstein, Y. M. Zhu, S. O'Brien, *J. Am. Chem. Soc.* **2005**, *127*, 9506.
[13] B. D. Yuhas, P. Yang, *J. Am. Chem. Soc.* **2009**, *131*, 3756.
[14] M. J. Siegfried, K.-S. Choi, *J. Am. Chem. Soc.* **2006**, *128*, 10356.
[15] C. G. Read, E. M. P. Steinmiller, K.-S. Choi, *J. Am. Chem. Soc.* **2009**, *131*, 12040.
[16] J. J. Teo, Y. Chang, H. C. Zeng, *Langmuir* **2006**, *22*, 7369.
[17] W. J. Tomlinson, J. Yates, *J. Phys. Chem. Solids* **1977**, *38*, 1205.
[18] T. L. Mokari, M. J. Zhang, P. D. Yang, *J. Am. Chem. Soc.* **2007**, *129*, 9864.
[19] N. Cabrera, N. F. Mott, *Rep. Prog. Phys.* **1949**, *12*, 163.
[20] Q. Darugar, W. Qian, M. A. El-Sayed, M. P. Pileni, *Journal of Physical Chemistry B* **2006**, *110*, 143.
[21] D. B. Pedersen, S. L. Wang, S. H. Liang, *Journal of Physical Chemistry C* **2008**, *112*, 8819.
[22] G. H. Chan, J. Zhao, E. M. Hicks, G. C. Schatz, R. P. Van Duyne, *Nano Letters* **2007**, *7*, 1947.
[23] W. Siripala, A. Ivanovskaya, T. F. Jaramillo, S. H. Baeck, E. W. McFarland, *Sol. Energy Mater.* **2003**, *77*, 229.
[24] E. Bundgaard, F. C. Krebs, *Sol. Energy Mater.* **2007**, *91*, 954.

Room-temperature Formation of Hollow Cu_2O Nanoparticles

By *Ling-I Hung*, *Chia-Kuang Tsung*, *Wenyu Huang*, and *Peidong Yang**

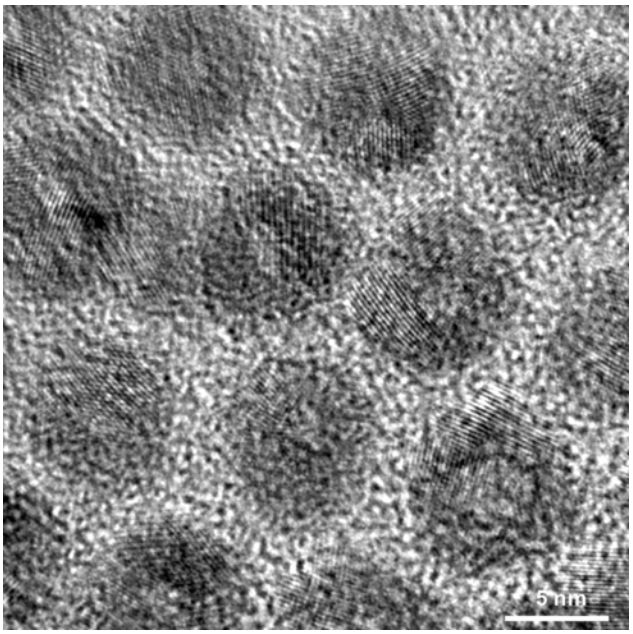

Figure 1S. HRTEM image of polycrystalline Cu_2O hollow NPs.

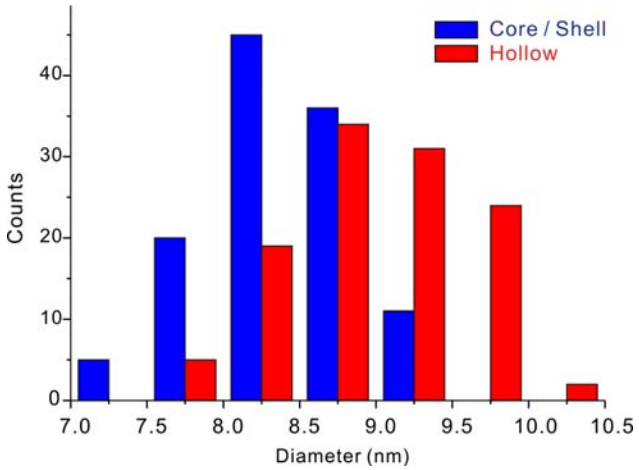

Figure 2S. Particle size distribution analysis during the oxidation process.

Acknowledgements: This work was supported by the Director, Office of Science, Office of Basic Energy Sciences, Material Sciences and Engineering Division, of the U.S. Department of Energy under Contract No. DE-AC02-05CH11231. We thank the National Center for Electron Microscopy for the use of their facilities.